SIMULATION AND VERIFICATION OF CORN WEEDING DEVICE BASED ON MACHINE VISION
/
基于机器视觉的玉米株间除草装置仿真及验证

Liu-xuan MA*[1)], kun TIAN[1)], Yi-lin WANG[1)], Shu-lin ZHANG[1)], Hao SUN [1)]
College of Mechanical Engineering, Jiamusi University, Jiamusi, Ha'erbin/ China
Tel: +86-17861501382; E-mail: tiankunsdau@163.com
DOI: https://doi.org/10.35633/inmateh-77-123

Keywords: *agricultural machinery, intra-row weeding, contact parameters, EDEM, tool resultant force*

ABSTRACT

This paper designs a maize interplant weeding machine to address issues like high seedling injury, low efficiency, and excessive tool stress in corn weeding. Using MATLAB, parameter optimization for plant spacing, protection zone radius, and tool radius results in a maximum weeding area coverage of 78.69%. Trajectory analysis improves adaptability in complex environments. A soil trough model based on EDEM identifies key factors affecting tool stress, with weeding depth having the greatest impact. The optimized parameters—plant spacing of 250 mm, weeding depth of 62 mm, and forward speed of 0.25 m/s—achieve 86.06% weeding rate and 2.76% seedling injury.

摘要

本文设计了一种玉米株间除草机，以解决玉米除草中苗伤率高、效率低、工具应力过大的问题。通过MATLAB优化株距、保护区半径和工具半径，最大除草覆盖率达到 78.69%。轨迹分析提高了机器在复杂环境中的适应性。基于EDEM的土壤槽模型揭示了影响工具应力的关键因素，其中除草深度对应力影响最大。优化后的参数—株距250mm、除草深度62mm、前进速度0.25m/s—实现了86.06%的除草率和2.76%的苗伤率。

INTRODUCTION

Maize is one of the major grain crops in northern China, and by the end of 2024 its national planting area reached 44,740.7 thousand hectares, accounting for 44.54% of all grain crops, with a total output of 294.917 million tons (NBS, 2023). However, weeds significantly affect maize yield by competing with seedlings for water, nutrients, and space, especially under high-temperature conditions due to their large root systems and species diversity *(Du et al., 2024; Wang et al., 2024; Zhang et al., 2023; Nosratti I et al., 2024)*. Weeding is therefore a critical operation during the maize growth cycle, also improving soil aeration, increasing surface temperature, and promoting seedling development *(Jia et al., 2020; Gobor et al., 2013)*.

In recent years, research on inter-row mechanical weeding has become relatively mature *(Zhang et al., 2021)*, but studies on intra-row weeding mechanisms remain limited and mainly rely on experimental testing, with room for improvement in weeding performance *(Leblanc et al., 2006; Ye et al., 2024)*. Li Linhong applied binocular cameras and YOLOv4 technology to accurately identify wolfberry plants and achieve autonomous navigation, improving robotic weeding usability *(Li et al., 2023)*. Haff developed an X-ray-based intra-row weeding system capable of identifying tomato stems with 90.7% accuracy at 1.6 km/h *(Haff et al., 2009)*. Zhang Chun long optimized a notched-blade intra-row weeding tool and identified the optimal parameters of 140° notch angle and 87.5 mm radius, achieving a weeding rate of 88.5% with low seedling damage *(Huang et al., 2014)*. Hu Lian used photoelectric sensors to obtain plant position information and guide a claw-type oscillating weeding mechanism, achieving a seedling-damage rate below 8% when spacing exceeded 20 cm *(Hu et al., 2012)*. Yu Changchang designed a vineyard trellis weeding machine with automatic width adjustment and obstacle avoidance, achieving 90.02% coverage and dual-side operation *(Yu et al., 2019)*. Zhang Zhien developed a cam-motion-based intra-row weeding device for lettuce, achieving a mean weeding rate of 91.09% *(Zhang et al., 2023)*. Zhao Xu investigated shear characteristics of maize root–soil composites through simulations and found soil moisture to be the most significant factor affecting ultimate shear stress *(Zhao et al., 2013)*.

[1] *Liuxuan MA*, Professor(Corresponding author);Kun TIAN, Master Degree; Yilin WANG, Experimental Technician; Shulin WANG, Senior Experimental Technician; Hao SUN, Master Degree;*

MATERIAL AND METHODS

CYCLOIDAL WEEDING DEVICE STRUCTURE AND WORKING PRINCIPLE

The structure of the visual interplant weeding device is shown in Figure 1 (actual device photo). It mainly consists of a visual recognition mechanism, weeding tool mechanical mechanism, and leveling mechanism. The stepper motor is connected to the slide rail through a plum blossom coupling, and a DC motor is installed on the slider to control the rotation of the weeding tool. The stepper motor is connected to the stepper motor controller, which is linked to the microcontroller, and further connected to the camera module and computer processing unit.

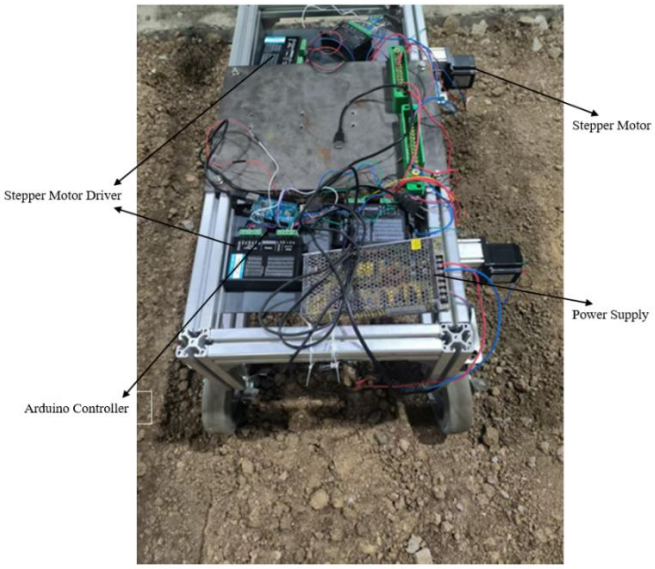

Fig. 1 – Corn Interplant Weeding Device

Initial Setup and Image Acquisition: At the start of the operation, the weeding device was in its preset initial state, with the camera precisely aligned with the center line of the crop row. Two sets of weeding tools were positioned at the extreme ends of the slide rail: the first set was at the far left, and the second set was at the far right. The monocular camera was mounted at the front of the device, with the following positional parameters: 100 cm height above the bed surface (adjustable), 30 cm horizontal distance from the first set of tools, and 80 cm from the second set of tools. During operation, a speed synchronization mechanism ensured that the camera captured a high-definition image of the plants on the bed every 10 cm of forward movement. This interval design prevented plant oversight, ensuring overlap between adjacent images based on the actual plant spacing, which was approximately 25 cm. With a 10 cm capture interval, even with slight variations in plant spacing, any plants missed in one image were captured in subsequent ones. The adjustable camera height allowed the horizontal field of view to expand with greater height, ensuring flexibility in the camera's range. Even at the lowest setting, the 10 cm interval guaranteed sufficient image overlap to reliably cover plant positions.

Real-time Image Processing and Decision-making: The captured images are transmitted in real-time to the host computer for processing. The core image processing task is to calculate the plant spacing between adjacent crops *(Kunz et al., 2018; Yang et al., 2018)*. Using image recognition technology, the center positions of each plant are accurately identified, and the trajectory equation is constructed on the host computer to avoid the protected zones (areas to be bypassed by the tools). The image processing algorithm is highly efficient; the YOLOv5 algorithm typically processes agricultural crop images at 150-250 ms per image *(Liang et al., Assirelli et al., 2018)*. However, the algorithm used in this device reduces the processing time to 70 ms, only 28%-47% of the average processing time of YOLOv5, enabling the device to perform weeding operations without delay.

Tool Movement Control and Collaborative Operation: Due to the 30 cm horizontal distance between the camera and the first set of tools, the host computer had sufficient time (determined by the distance from the camera to the tools and the device's forward speed) to plan the obstacle avoidance path for the first set of tools. Similarly, the 80 cm distance between the camera and the second set of tools provided a longer time window for processing and response. The host computer calculated the required lateral obstacle avoidance movement trajectory for the tools, considering the device’s speed and the real-time position information of adjacent plants. Control instructions were sent to the microcontroller system, which generated pulse signals to drive the stepper motor and precisely controlled the lateral movement of the tools along the slide rail.

The combined movement resulted in a cycloidal trajectory traced by the tool tip, closely approximating the ideal path. The weeding tools rotated continuously under the stepper motor's control, with the blades cutting into the soil following the cycloidal path, effectively severing the weed roots and slightly disturbing the surface soil structure. Weeds and soil clumps in the tool's path were loosened and detached due to the loss of adhesion to the soil. The loosened weeds and soil were then separated by the device's soil-breaking mechanism, completing the weeding operation.

The dynamically generated plant protection zones ensured that the tools efficiently weeded while avoiding plant damage, significantly reducing seedling injury rates. By optimizing the cycloidal path and combining real-time sensing and decision-making, the system effectively increased the coverage rate of weed removal between rows and between plants. The automated image recognition, real-time decision-making, and control greatly enhanced the efficiency and intelligence of the overall weeding operation.

Key component design and parameter determination

This study focused on interplant weeding machinery for maize at the seedling stage. Since maize was usually planted in late May to early June, when temperatures were higher, both maize and weeds grew rapidly, and weeds tended to occur in clusters. The peak weeding period typically occurred when maize reached the 3- to 5-leaf stage, which was also the critical period for weed management (*Jia et al., 2021*). At this stage, the maize's main root system began to thicken, and some secondary roots (permanent main roots derived from underground stem nodes) started to grow. These roots, located in the soil's surface layer, were distinctly different from the roots of weeds during the same period, allowing for optimal weeding efficiency. Additionally, maize images at the 3- to 5-leaf stage showed significant differences from weeds, providing better results during subsequent image dataset training. Based on this, this study selects this stage for operation. According to the measurement data from the Jiamusi University Experimental Canter's soil trough base, the maize root depth h_2 is approximately 10-20 cm, plant height H_2 is 15-30 cm, plant spacing H_1 is 20-30 cm, and row spacing H_3 is 50-70cm. Weed root length h_1 is generally 5–10 cm after about 15 days, and the plant diameter is around 1 cm. The field environment for interplant weeding in maize is shown in Figure 2. Modern agricultural machinery components such as tools, wheel tracks, and sensors are designed according to standard row spacing. Although slight variations in row spacing may exist, the agricultural machinery can compensate for deviations automatically through the auto-navigation system and flexible adjustment mechanisms to ensure operational accuracy. The research team from China Agricultural University reported that, during navigation trials of a maize weeding robot, the standard deviation of the lateral offset of plant centers at the V3 growth stage (third leaf fully expanded) ranged from 1.2 to 2.8 cm (maximum < 3 cm). This deviation was primarily attributed to seed drill vibration and soil loosening during the seedling emergence period *(Lai et al., 2023)*. Since the deviation value is smaller than the protection zone range, the plant's center remains within the protection zone, albeit with some deviation at the protection zone's location (illustrated in Figure 4 of the subsequent sections). Therefore, this study did not consider row spacing deviations.

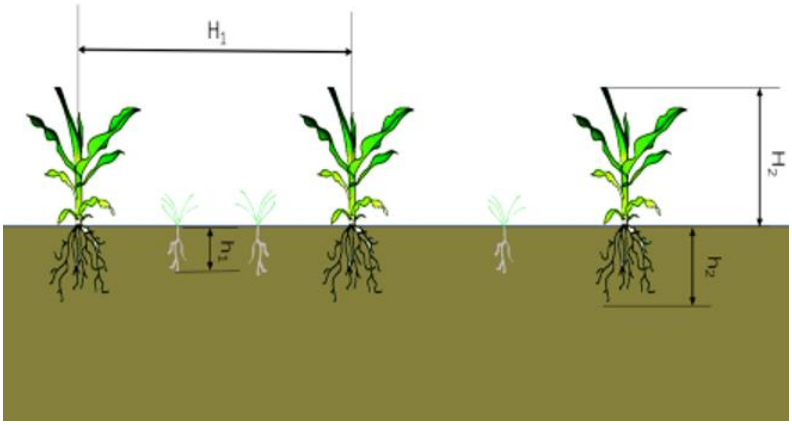

Fig. 2 – Field Environment for Maize Weeding

According to the design principles of the weeding device, the main factors affecting the weeding rate and seedling injury rate were the protection zone radius, tool radius, and tool depth. Compared to traditional interplant weeding devices, the cycloidal weeding device offered several advantages: its speed curve was continuous and differentiable, making it easier for the controller to track the trajectory and reducing overshoot

or delay. The power demand was smooth, preventing instantaneous motor overloads, thereby reducing energy consumption and heat generation. Additionally, the stress variation on the components was gradual, which helped to reduce material fatigue.

Based on the field survey of the maize row spacing, in order to minimize the seedling injury rate while maximizing the weeding area:

$$\begin{cases} y_1 = (r_1 + r_2)\cos\left(\dfrac{\pi x}{a}\right) - r_2 \\ y_2 = (r_1 + r_2)\cos\left(\dfrac{\pi x}{a}\right) + r_2 \end{cases} \quad (1)$$

a is the plant spacing between two adjacent plants (mm); r_1 is the set protection zone radius (mm); r_2 is the weeding tool radius (mm); y_1 is the tool boundary trajectory function 1; y_2 is the tool boundary trajectory function 2.

After defining the tool trajectory equation, the subsequent step is to calculate the weeding omission area.

$$\begin{cases} S_1 = \int_0^{\frac{\pi}{a}\cos^{-1}\left(\frac{r_2}{r_1+r_2}\right)} y_1 dx - \dfrac{1}{4}\pi r_1^2 \\ S_2 = \dfrac{a}{2}(r_1 + 2r_2) - \int_0^{\frac{a}{2}} y_2 dx \\ S = S_1 + S_2 \\ B = \dfrac{S}{\dfrac{a}{2}(r_1 + 2r_2)} \end{cases} \quad (2)$$

In the above equation: S_1 is the weeding omission area near the protection zone; S_2 is the boundary omission area; S is the total omission area; and B is the weeding area omission rate.

Using MATLAB to analyze the impact of three parameters on S .The following figure illustrates the impact of parameters on S.

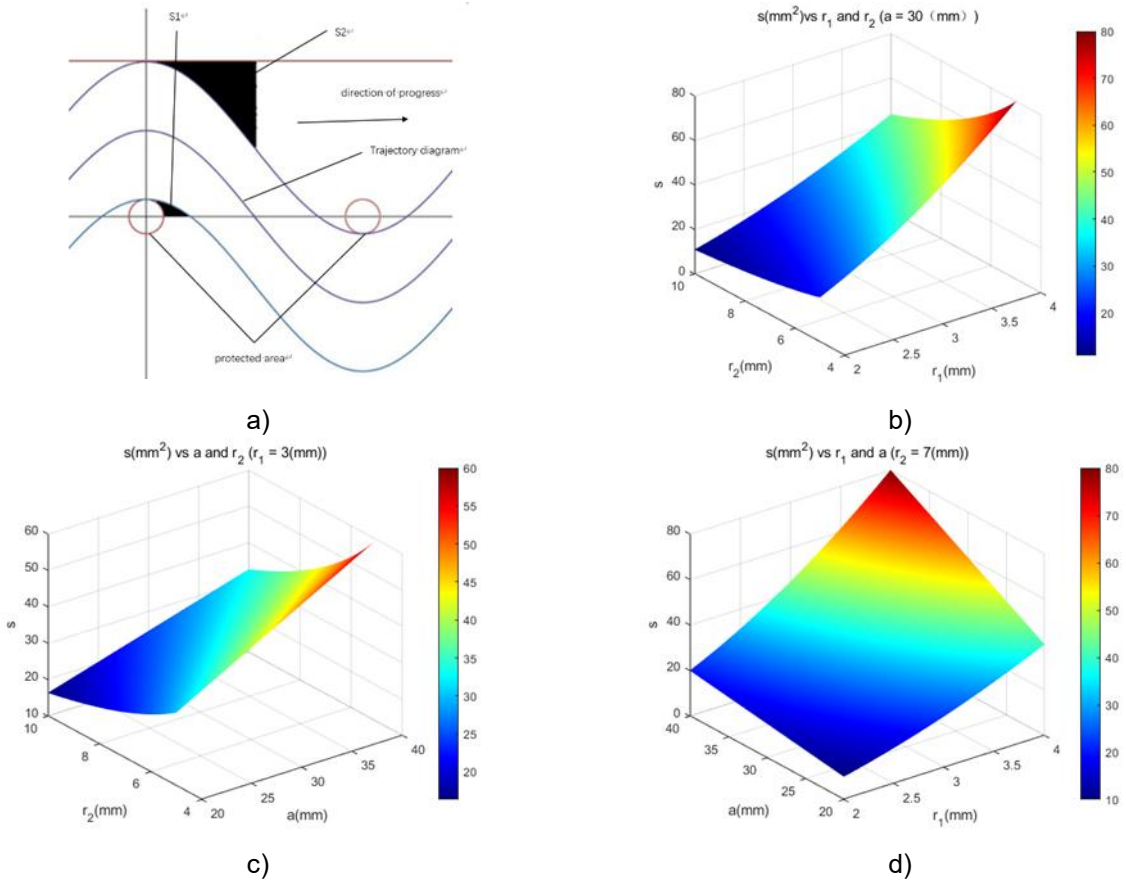

Fig. 3 – The relationship between weeding omission area and various factors

To achieve the minimum omission area rate (maximum weeding area coverage rate) and to ensure that the protection zone was not encroached upon, the tool radius, protection zone radius, and plant spacing during planting were determined. This study used MATLAB to analyze the scenario where the adjacent plant spacing was a (ranging from 10-30 cm), the protection zone radius is r_1 (3-4 cm), and the tool radius is r_2 (4-8 cm). By fixing one of the three factors, the effects of the other two factors on the operational indicators were examined to determine the value range and level division of each factor, providing a theoretical basis for the subsequent soil trough experiments. Where a represented the motion trajectory and omission area, and b, c, and d represented the effects of the remaining two parameters on experimental indicators after fixing the plant spacing, protection zone radius, and tool radius parameters. Simulation results showed that when the plant spacing was 15.5 cm, the protection zone radius was 3.98 cm, and the tool radius was 7.95 cm, while ensuring the tool did not encroach on the protection zone (as shown in Equation 3), the maximum weeding area coverage rate was 78.74%. In subsequent practical situations, with a plant spacing of 155 mm, protection zone radius of 40 mm, and tool radius of 80 mm, and ensuring that the tool did not intrude into the protection zone, the maximum weeding area coverage rate was 78.69%.

To ensure that the tool did not encroach on the protection zone, as shown in Equation (3), the minimum curvature of the trajectory had to be greater than the curvature of the protection zone, satisfying the requirement that the tool did not invade the protection zone.

$$\begin{cases} k_{curve} = \dfrac{\pi^2 (r_1 + r_2)}{a^2} \approx 1.027 \\ k_{circle} = \dfrac{1}{r_1} \approx 0.251 \\ k_{curve} = 1.027 > k_{circle} = 0.251 \end{cases} \quad (3)$$

Weeding tool motion trajectory analysis

To achieve flexible movement of the weeding tool between plants, a stepper motor was used for control. The stepper motor offered advantages such as high precision, quick response, and low cost, making it well-suited for complex field environments. The rotation speed was adjusted in real-time by changing the pulses. The weeding action directly affected the weeding tool's movement range in the field, which in turn impacted the effectiveness of weed removal. During weeding operations in the field, the maize root system growth often influenced the work. To minimize the impact of the tool on the maize roots, this study linked the weeding mechanism to the slide rail. By constructing a system that included a plant protection zone, a reciprocating variable speed motion of the tool along the slide rail was formed. Combined with a constant forward speed of the device, this resulted in a cycloidal weeding operation. This significantly improved the work efficiency of the interplant weeding mechanism. Compared to other methods, this approach was simple and efficient, and it could effectively move between plants without causing excessive seedling damage.

Trajectory with fixed plant spacing on one side of the maize

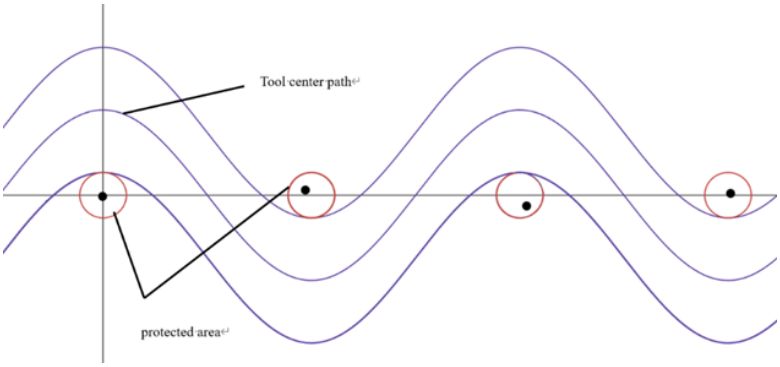

Fig. 4 – Cycloidal Trajectory with Fixed Plant Spacing

Note: The black marks in the figure represent the possible actual maize plant positions, and the curve in the figure represents the weeding trajectory as given by Equation (4).

$$y = A\cos(\omega t + \varphi) \tag{4}$$

$$x = vt \tag{5}$$

Given that the period of the curve in the previous section is $2a$, the following formula (6) applies;

$$2a = T = \frac{2\pi}{\omega} \tag{6}$$

where: T - the period of the tool trajectory function; A- the amplitude of the trajectory function; v - forward speed of the device. From formulas (4), (5), and (6), formula (7) can be derived:

$$y = A\cos(\omega t) \tag{7}$$

By differentiating formula (7) with respect to time, the formula for the lateral movement speed, formula (8), can be obtained:

$$v_y = A\frac{\pi}{a}\sin(\frac{\pi x}{av}) \tag{8}$$

$$v_y = -1^{\left\lfloor \frac{x}{a} \right\rfloor} A\frac{\pi}{a}\sin\left(\frac{\pi x}{av}\right) \tag{9}$$

The above formula represents the speed formula for one side entering the plant zone. To ensure the continuity of the entire curve, a rounding function is added to the formula.

Trajectory during single-sided maize missed sowing

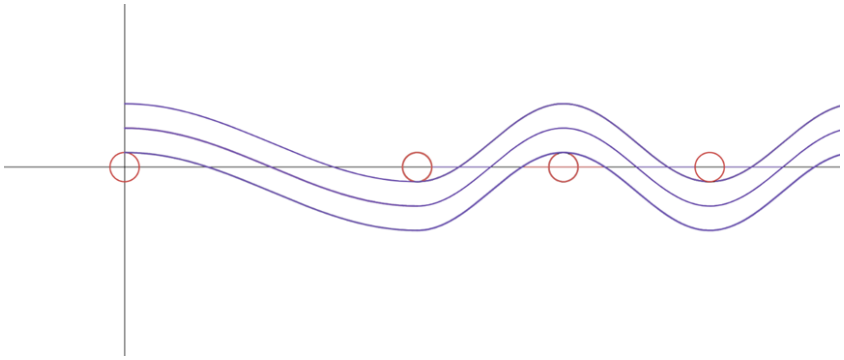

Fig. 5 – Trajectory during Single-Sided Maize Missed Sowing

When the computer detected that the plant spacing was greater than the originally set normal plant spacing, the tool's composite movement remained a cycloidal motion. However, at this point, the processing unit reconstructed the new trajectory equation based on the new plant spacing value and solved for the lateral displacement speed formula. The trajectory equation remained as formula (9).

Trajectory during single-sided maize reseeding

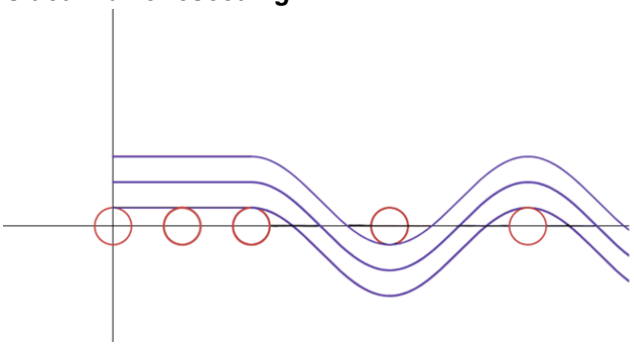

Fig. 6 – Trajectory during Single-Sided Maize Reseeding

When the computer detected that the actual plant spacing was too small, a plant protection zone was still created. If the adjacent plant spacing was less than 1.2 times the tool diameter, the operation did not enter the plant spacing area. Instead, the operation was carried out along the forward direction of the machine at the positions where the plant protection zone's upper and lower boundaries were tangent. At this point $v_y = 0$.

Discrete element method (DEM) and weeding tool simulation

When the weeding tool cut into the soil and weed roots, the tool generated additional torque to better penetrate the soil. To ensure that the tool could cut through the weed roots at the specified rotational speed, the shear force generated by the tool's rotation had to exceed the shear strength of the weed roots and soil. Therefore, DEM simulations were conducted to test the forces experienced by the tool under different plant spacing conditions. Since the discrete element model of the weed roots was quite complex and the tool resistance during soil operation mainly originated from the soil, a simplified representation of the weed root trunks was adopted. Later, the weeding effect was determined by assessing the tool's cutting performance on weed particles. A finite element analysis was added for the primary weed root systems, and an EDEM software-based DEM simulation model was built for the "tool-weed-soil" interaction. The soil's DEM model parameters were calibrated using slump test data. The material parameters of the soil model and weeding device were shown in the table below.

Table 1

Soil Model and Tool Parameter Calibration

Parameters	Value
soil Density(kg*m^3)	2680
Soil Particle Poisson's Ratio	0.38
Soil Particle Elastic Modulus	1e^6
Density/(kg*m^3)	7850
Poisson's Ratio	0.3
Shear Modulus/ MPa	2.1*10e^6
Coefficient of Static Friction	1
Coefficient of Rolling Friction	0.15
Coefficient of Restitution	0.5
Coefficient of Rolling Friction between Soil Particles and the Tool	0.2
Coefficient of Static Friction between Soil Particles and the Tool	0.4
Coefficient of Restitution between Soil Particles and the Tool	0.5

Based on the data in the table above, the EDEM particle model and material parameters were constructed. The Hertz-Middle in with JKR model, which was embedded in the software, was used for the interaction between particles, effectively simulating the cohesiveness of Northeast black soil. For other interactions, the Hertz-Middle (no slip) model was used. Based on a 13 mm equivalent particle diameter, Peng Cheng Wan Li determined the shape sizes for four types of soil particles: single ball, double ball, triple ball, and four-ball. Various packing methods, such as single ball, single ball with variable particle diameter, double ball, triple ball, four-ball, and multi-ball mixtures, were used to establish six virtual soil models. Subsequently, simulation tests on the plowing process were conducted with tillage resistance, post-tillage angle of accumulation, and simulation time as experimental indicators. The results showed that the relative error between the simulated and measured tillage resistance for the six virtual soil models was less than 8% *(Wan et al., 2021)*. Furthermore, using a single particle type can speed up the simulation process, which is beneficial for the simulation of tool resistance and reduces the amount of simulated data. The soil trough simulation model was constructed with dimensions of 600 mm * 460 mm * 180 mm. The 3D models of the tool and shaft, designed in Creo software, were imported into the EDEM pre-processor. The soil particles were selected to be spherical, the blade was set as structural steel, and the mesh size was set to 3R_min (where $R_{\min}$ is the minimum radius of the soil particles).

Simulation test method

During the weeding operation of the device, the forward speed was kept constant in the design, so the weeding depth and plant spacing had a significant impact on the tool resistance. Therefore, this study took weeding depth, forward speed, and adjacent plant spacing (which directly determined the magnitude and frequency of the tool's instantaneous speed adjustment in the y-axis direction during the weeding operation) as experimental factors. The resistance of the tool in the soil was used as the experimental indicator for the

orthogonal combination simulation test. The weeding depth was defined as the distance from the lowest point of the tool to the average height of the soil surface; plant spacing referred to the distance between two adjacent plants in the same row, and the forward speed was the speed of the device along the plant row. The experimental factor level coding table was shown below:

Table 2

Factor Level Coding Table

Codes	Row spacing $X1$ / mm	Weeding depth $X2$ / cm	Forward speed m/s
1	300	10	0.4
0	200	8	0.3
-1	100	6	0.2

The resultant force on the tool was calculated through post-processing in the EDEM software, as shown in Figure 7. During the operation of the mechanism, due to the particle generation and tool placement time in the initial seconds of the simulation, only the resultant force diagram of the tool after this period was exported, and the magnitude of the resultant force was recorded.

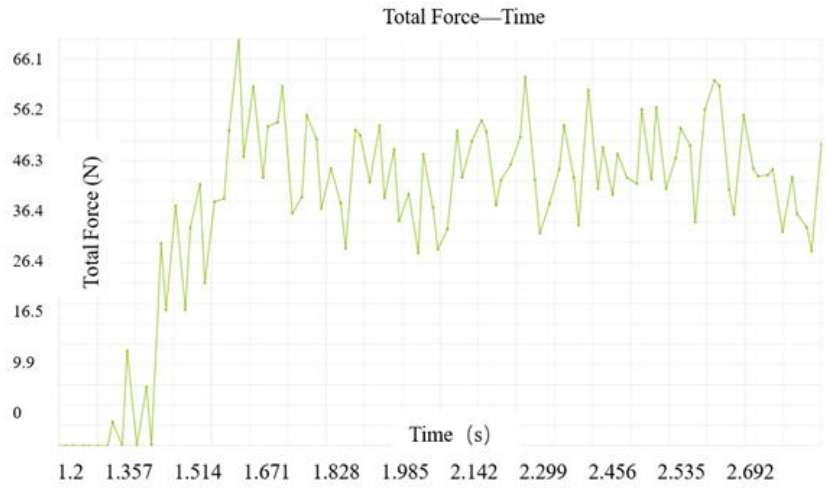

Fig. 7 – EDEM Simulation Post-Processing Interface

RESULTS

The secondary orthogonal experimental design and results were shown in Table 3. The pressure variance analysis and significance results were shown in Table 4. The experimental data and results from Table 3 were input into Design-Expert 13 software for regression analysis, establishing the regression equation between the experimental indicator resultant force and the experimental factors, as shown in the following equation:

$$Y = 46.78 - 2.69X_1 + 11.66X_2 + 7.73X_3 + 4.07X_1X_2 + 5.27X_2^2 \quad (10)$$

Table 3

Test Scheme and Results

Test Number	Plant Spacing x_1/(mm)	Weeding Depth x_2/(mm)	Forward Speed x_3/(m/s)	Total Force Y/(N)
1	100	60	0.3	47.5
2	300	60	0.3	34.1
3	100	100	0.3	63.2
4	300	100	0.3	66.1
5	100	80	0.2	42.8
6	300	80	0.2	37.3
7	100	80	0.4	58.6
8	300	80	0.4	53.1
9	200	60	0.2	34
10	200	100	0.2	56
11	200	60	0.4	48.3
12	200	100	0.4	71.9

Test Number	Plant Spacing x_1/(mm)	Weeding Depth x_2/(mm)	Forward Speed x_3/(m/s)	Total Force Y/(N)
13	200	80	0.3	46.8
14	200	80	0.3	46.3
15	200	80	0.3	47.2
16	200	80	0.3	46.6
17	200	80	0.3	47

(Note: x_1 is the coded value for plant spacing ; x_2 is the coded value for weeding depth; x_3 is the coded value for forward speed; Y is the magnitude of the tool resultant force.)

Table 4

Pressure Variance Analysis Table

Source		df	Mean Square	F-value	P-value	
Model	1814.12	9	201.57	1072.58	< 0.0001	significant
X1	57.78	1	57.78	307.46	< 0.0001	
X2	1088.11	1	1088.11	5790.03	< 0.0001	
X3	477.41	1	477.41	2540.35	< 0.0001	
X1×X2	66.42	1	66.42	353.45	< 0.0001	
X1×X3	0	1	0	0	1	
X2×X3	0.64	1	0.64	3.41	0.1075	
X_1^2	1.9	1	1.9	10.13	0.0154	
X_2^2	117.05	1	117.05	622.84	< 0.0001	
X_3^2	1.04	1	1.04	5.55	0.0507	
Residual	1.32	7	0.1879			
Lack of Fit	0.8275	3	0.2758	2.26	0.2235	not significant
Pure Error	0.488	4	0.122			
Cor Total	1815.44	16				

From the table, it could be seen that the model, adjacent plant spacing, weeding depth, forward speed, adjacent plant spacing × weeding depth, and the square of weeding depth had a significant impact on pressure magnitude. However, adjacent plant spacing × forward speed, weeding depth × forward speed, the square of adjacent plant spacing, and the square of forward speed did not significantly affect the pressure magnitude. Additionally, the Lack of Fit was not significant, indicating that the model fit well, was stable, and the experimental indicators could be analyzed using the regression model. Based on the F-values in the table, the influence rates of the factors on pressure magnitude were: weeding depth > forward speed > adjacent plant spacing.

Using Design-Expert 13 software, a response surface analysis of the experimental results was performed, and the results were shown in Figure 8.

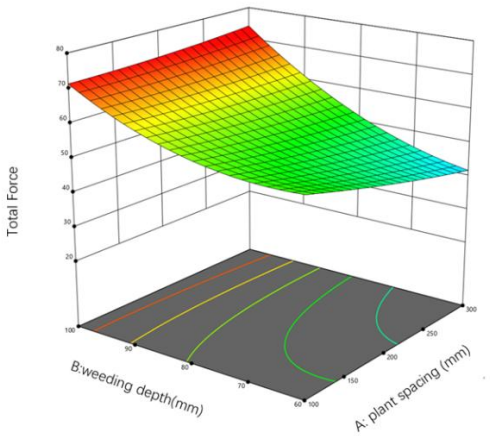

Fig. 8 – Response Surface

Adjacent plant spacing and weeding depth had an impact on pressure. From the figure, it could be seen that the maximum pressure increased with the increase in weeding depth. When the plant spacing was less than 200 mm, the range of change in maximum pressure gradually decreased as weeding depth increased. When the plant spacing was greater than 200 mm, the increase in plant spacing caused a more significant increase in maximum pressure. Maximum pressure increased with weeding depth, and when the weeding depth was less than 80 mm, the trend of maximum pressure decreasing with increasing plant spacing became significantly larger. When the weeding depth was greater than 80 mm, the range of change in maximum pressure decreased significantly.

Using Design-Expert software to optimize the indicators, the optimization goal was to minimize the maximum pressure on the tool. The best combination of experimental factors obtained from the analysis was a plant spacing of 257.281 mm, weeding depth of 62.339 mm, and a forward speed of 0.244 m/s. At this point, the maximum pressure was 33.268 N. To ensure the feasibility of future work, the parameters were rounded. The optimal weeding parameters were rounded to a plant spacing of 250 mm, weeding depth of 62 mm, and forward speed of 0.25 m/s. The best weeding plant spacing was 70% of this value, which was 175 mm, slightly larger than the theoretical minimum plant spacing from the MATLAB experiment (below 155 mm, the tool would intrude into the protection zone).

Experimental verification results

To verify the optimized parameters, an experimental field was set up. A colored circular ring with a radius of 3 cm was used to replace the protection zone. Before transplanting, the soil was rototilled and leveled, and the bed ridges were constructed. The weed species selected for the experiment were Amaranthus retroflexus and Portulaca oleracea, which were randomly distributed across the experimental field. The weeding tool was set at a depth of 62 mm, and the forward speed was selected as 0.25 m/s. Figure 9 showed the layout before and during the operation of the equipment. In the figure, (a) showed the field before weeding, (b) showed the field after weeding, and (c) showed the watering treatment applied to deepen the weeding trajectory.

a) b) c)

Fig. 9 – Comparison of the Equipment Before and After Operation

Five verification experiments were conducted, and the weeding rate and seedling injury rate for each experiment were statistically analyzed to obtain the average value. The formula for calculating the seedling injury rate is:

$$S = \frac{N - M}{N} \times 100\% \tag{11}$$

In the equation, S is the weeding rate of the weeding machine (%); N is the number of weeds in the experimental field before weeding; M is the remaining number of weeds in the experimental field after weeding. The seedling injury rate formula is as follows:

$$I = \frac{N - M}{N} \times 100\% \tag{12}$$

In the equation, I is the seedling injury rate of the weeding machine (%); L is the number of colored rings before weeding; H is the number of instances where the tool intrudes into the protection zone. The experimental results are shown in Table 5.

Table 5

Results of Five Field Experiments

Experiment ID	Weed Control Efficacy (%)	Seedling Damage Rate (%)
1	85.6	2.8
2	84.7	2.6
3	86.9	1.9
4	88.7	2.3
5	84.4	4.2
Mean	86.06	2.76

In the test operations in the experimental field, the maize interplant weeding device achieved an average weeding rate of 86.06% and an average seedling injury rate of 2.76% when the forward speed was 0.25 m/s, plant spacing was 250 mm, and weeding depth was 62 mm. The experimental results indicate that the cycloidal maize interplant weeding machine meets the agronomic requirements for weeding rate and seedling injury rate.

CONCLUSIONS

A maize interplant weeding machine based on cycloidal oscillation was designed. The analysis showed that the device could successfully perform weeding under variable plant spacing conditions without damaging the crops. MATLAB simulations determined the optimal tool and protection zone radii (155 mm plant spacing, 40 mm protection zone, 80 mm tool), achieving a maximum weeding coverage rate of 78.7%. Discrete element method (DEM) simulations combined with orthogonal tests revealed that weeding depth was the main factor affecting the resultant force on the tool, followed by forward speed and plant spacing. Response surface optimization provided the best operational parameters: plant spacing of 250 mm, weeding depth of 62 mm, and forward speed of 0.25 m/s, which minimized the maximum resultant force in the simulation. In five field tests, the machine using these parameters achieved an average weeding rate of 86.06% and a seedling damage rate of 2.76%, validating the effectiveness of the calculated results.

REFERENCES

[1] Assirelli A., Liberati P., Santangelo E., Del Giudice A., Civitarese V., Pari L. (2015). Evaluation of sensors for poplar cutting detection to be used in intra-row weed control machine [J]. *Computers and Electronics in Agriculture*, 115: 161-170.

[2] Du Yagang, Zhang Yu, Sui Xin, Dai Hongfei. (2024). Research Progress on Corn Weeding Machinery and Technology[J](玉米除草机械及技术研究进展). *Agricultural Development & Equipment*, (12): 49-51.

[3] Gobor Z., Lammers P.S., Martinov M. Development of a mechatronic intra-row weeding system with rotational hoeing tools: Theoretical approach and simulation[J]. *Computers and Electronics in Agriculture*, 2013, 98: 166-174.

[4] Haff, R.P., & Slaughter, D.C. (2009). X-ray based stem detection in an automatic tomato weeding system. *2009 Reno*, Nevada, June 21 - June 24, 2009.

[5] Hu Lian, Lin Chaoxing, Yang Weiwei, Xu yi. (2014). Design of Control System for Switching between Weeding and Seedling Avoiding States of Intra-Row Weeding Device [J] (株间除草装置的除草和避苗状态切换控制系统设计). *Journal of Shenyang Agricultural University*, 45(03): 305-309.

[6] Hu Lian, Luo Xiwen, Zhang Zhigang, Chen Xiongfei. (2012). Seedling avoidance control algorithm for intra-row mechanical weeding claws based on trochoid motion[J](基于余摆运动的株间机械除草爪齿避苗控制算法). *Transactions of the Chinese Society of Agricultural Engineering*, 28(23): 12-18.

[7] Huang Xiaolong. (2014). *Optimization Design Research on End Effector of Intra-Row Weeding Robot for Vegetables [D](蔬菜株间锄草机器人末端执行器优化设计研究)*. China Agricultural University,

[8] Jia H.L., Gu B.L., Ma Z.Y., Liu H.L., Wang G. (2021). Optimized design and experiment of spiral-type intra-row weeding actuator for maize (Zea mays L.) planting[J]. International Journal of Agricultural and Biological Engineering, 14(6): 54-60.

[9] Jia H, Gu B, Ma Z . (2021). Optimized design and experiment of spiral-type intra-row weeding actuator for maize (Zea mays L.) planting [J]. *International Journal of Agricultural and Biological Engineering*, 14(6): 54-60.

[10] Kunz C, Weber J F, Peteinatos G, Sokefeld M , Gerhards R. (2018). Camera steered mechanical weed control in sugar beet, maize and soybean[J]. *Precision Agriculture*, 19(4): 708-720.

[11] Lai Hanrong, Zhang Yawei, Zhang Bin, Yi Yanxin, Liu Yuahng. (2023). Design and experiment of visual navigation system for corn weeding robot[J](玉米除草机器人视觉导航系统设计与试验). *Transactions of the Chinese Society of Agricultural Engineering*, 39(01): 18-27.

[12] LeBlanc M.L., Cloutier D.C., Stewart K.A. (2006). Rotary hoe cultivation in sweet corn[J]. *Hort technology*, 16(4): 583-589.

[13] Li Linhong. (2023). *Research on Key Technologies of Autonomous Mobility and Precise Identification and Positioning for Intra-Row Weeding Robot in Wolfberry Orchard* (枸杞园株间除草机器人自主移动与精准识别定位关键技术研究) [D]. Ningxia University;

[14] Liang Yun. (2018). *A Weeding Device for Corn Intra-Row Weeder. Patent. CN207783465U*[P](一种用于玉米株间除草机的除草装置). China

[15] Nosratii I, Sabeti P, Chaghamirzaee G, Heidari H. (2020). Weed problems, challenges, and opportunities in Iran[J]. *Crop Protection*, 134.

[16] Wang Wei, Sun Mingzhe, Zhang Dingtong, Xu Haibo, Liu Siyan. (2024). Design and Experiment of Dry Field Mechanical Weeder[J](旱田机械除草机的设计与试验). *Southern Agricultural Machinery*, 55(17): 30-33.

[17] Wanli Pengcheng, Li Yonglei, Su Chen, Zhao Hu, Dong Xiangqian. (2021). Simulation of Soil Tillage Characteristics Based on EEPA Contact Model and Analysis of Particle Sphere Influence[J](基于 EEPA 接触模型的土壤耕作特性模拟及颗粒球型影响分析). *Journal of China Agricultural University*, 26(12): 193-206.

[18] Yang Guangyou, Zhang Qiang, Ma Zhiyan, (2018). *An Agricultural Robot for Intra-Row Weeding*. Patent. No. CN208402489U. China

[19] Ye Sheng Hao. (2024). *Design and Experimental Study on Intra-Row Weeding Device for Soybean (大豆株间除草装置的设计与试验研究)* [D]. Chinese Academy of Agricultural Sciences,

[20] Yu Changchang, Xu Liming, Wang Qingjie, Yuan Quanchun, Ma Shuai. (2019). Design and Experiment of Automatic Obstacle Avoidance Intra-Row Weeder for Bilateral Operation in Hedge-trained Vineyard[J](篱架式栽培葡萄双边作业株间自动避障除草机设计与试验). *Transactions of the Chinese Society of Agricultural Engineering*, 35(05): 1-9.

[21] Zhang Denghong, Xiao Chunfang, Wang Zhen, Zhang Xueyuan, Shen Yanfen. (2023). *Research on Small Machinery for Vine Killing and Weeding in Potato Fields*[C](马铃薯田小型机械杀秧除草研究)// Chinese Crop Society Potato Professional Committee, Heilongjiang Provincial Department of Agriculture and Rural Affairs, Qiqihar Municipal People's Government, Beidahuang Agricultural Reclamation Group Co., Ltd. Potato Industry and Seed Industry Innovation Hubei Enshi China Southern Potato Research Center; Enshi Tujia and Miao Autonomous Prefecture Academy of Agricultural Sciences, 2023: 255-257.

[22] Zhang Jingyu (2021). *Design and Experiment of Intelligent Intra-Row Mechanical Weeding Device for Ridge-planted Corn (垄作玉米智能株间机械除草装置设计与试验)* [D]. Northeast Agricultural University,

[23] Zhang Zhien (2023). *e*[D]. Zhejiang Sci-Tech University,

[24] Zhao Xu, Zhang Zuli, Huang Qiubo, Zhang Guoliang. (2013). Experiment on Shear Performance of Corn Root-Soil Composite[J](玉米根土复合体剪切性能试验). *Transactions of the Chinese Society for Agricultural Machinery*, 44(08): 126-132.

[25] ***National Bureau of Statistics. Announcement on Grain Output Data in 2024[Announcement], 2023-12-13.